Vanadium-51 MAS and Static NMR Studies of the Binary V_2O_5−WO_3 System

Becky A. Gee* and Anna Wong†

Department of Chemistry and Biochemistry, Long Island University-Brooklyn Campus, Brooklyn, New York 11201

Received: March 28, 2003

Solid-state NMR spectra showing single-quantum excitation of the vanadium-51 ($I = 7/2$) central and six satellite transitions were obtained for polycrystalline V_2O_5 and $x\%V_2O_5$−$(100 - x\%)WO_3$ (10 mol % ≤ x ≤ 40 mol %) solids by magic angle spinning (MAS) and static NMR spectroscopies. All MAS spectra show full spinning sideband manifolds resulting from incomplete averaging of the chemical shift and quadrupolar interaction anisotropies. Chemical shift parameters (δ_{iso}, δ_{aniso}, η_{cs}) and quadrupolar parameters (C_Q, η_Q) were obtained by simulation of both MAS and static spectra. A single vanadium site was observed in the nominally 40 mol % V_2O_5−60 mol % WO_3 and 30 mol % V_2O_5−70 mol % WO_3 compositions. Interpretation of NMR spectral parameters suggests that the vanadium in this single site resides in a square pyramid-like oxygen coordination environment. Three sites were observed for the nominally 20 mol % V_2O_5−80 mol % WO_3 and 10 mol % V_2O_5−90 mol % WO_3 compositions. The spectral parameters for the three sites are consistent with the presence of vanadium(V) in (1) square pyramid-like, (2) distorted tetrahedral, and (3) spherically symmetric oxygen coordination environments. A distribution of ^{51}V quadrupolar coupling parameters may be present and may suggest a distribution of second or higher order atomic environments.

Introduction

Vanadium and tungsten oxides have drawn attention in the literature because of their current and conceivable technological applications. Supported vanadium oxide based catalysts are particularly versatile in their ability to reduce nitrogen oxides in the presence of ammonia, oxidize sulfur dioxide, and oxidize several hydrocarbons. In particular, vanadia supported on titania has proven to be an industrially important material for the selective catalytic reduction (SCR) of nitrogen oxides (NO_x) that originate from the combustion of fossil fuels.[1,2] Recent work has provided evidence for the enhanced catalytic performance of tungsten oxide promoted V_2O_5/TiO_2 for the SCR of nitric oxide. More recently, the properties of mixed vanadium tungsten oxide thin films have been investigated in light of their potential use in electrochromic devices.[3]

The structure of vanadium pentaoxide has been refined in the orthorhombic (*Pmmn*) space group.[4] There are six nearest neighbor oxygen atoms at variable distances from each vanadium atom in the structure (Figure 1). Four oxygens are each nearly equidistant from the central vanadium atom forming a distorted square planar coordination environment, while the two axial oxygens are at distances of 1.577 and 2.791 Å from the central vanadium atom. Each polyhedron shares two edges and two corner planar oxygens with four neighboring polyhedron with the short axial V−O bond alternating its position by 180° between adjacent polyhedra. Each polyhedron in the corner/edge shared layer then corner shares its axial oxygens with vanadium atoms below and above its layer.

The structure of WO_3 is similar to that of the perovskite $CaTiO_3$ (ABO_3) structure type with B-type cations located at corners of the unit cell and oxygen atoms at each edge thus forming a three-dimensional lattice of corner-sharing octahedra. In the ABO_3 compounds, the larger A cation is coordinated by 12 oxygens atoms and is located at the center of the unit cell while the A site is unoccupied in the WO_3 structure. The room-temperature WO_3 structure (monoclinic, $P2_1/c$) differs from the ideal cubic perovskite for the oxygen atoms form distorted and tilted octahedra and the tungsten atoms are situated off center (Figure 2).[5] Tungsten trioxide undergoes facile crystallographic transitions near room temperature, and thus several WO_3 polymorphs exist in addition to the ABO_3 structure type.

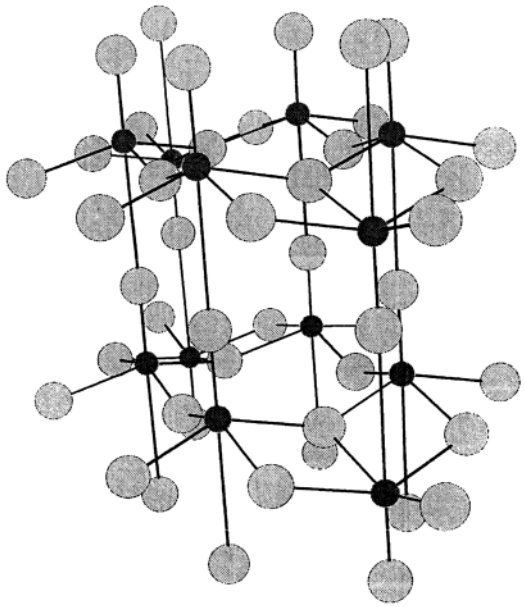

Figure 1. V_2O_5 structure. Vanadium atoms are shown in black and oxygen atoms are depicted in gray. (Not a unit cell.)

Previous structural studies of bulk V_2O_5−WO_3 have provided useful insights. However, the structure of bulk V_2O_5−WO_3

* Corresponding author. E-mail: bgee@liu.edu. Phone: 718 246 6397. Fax: 718 488 1465.

† Intel Science Talent Search Student (Bronx High School of Science Class of 2002, New York City).

10.1021/jp030379m CCC: $25.00
Published on Web 07/19/2003

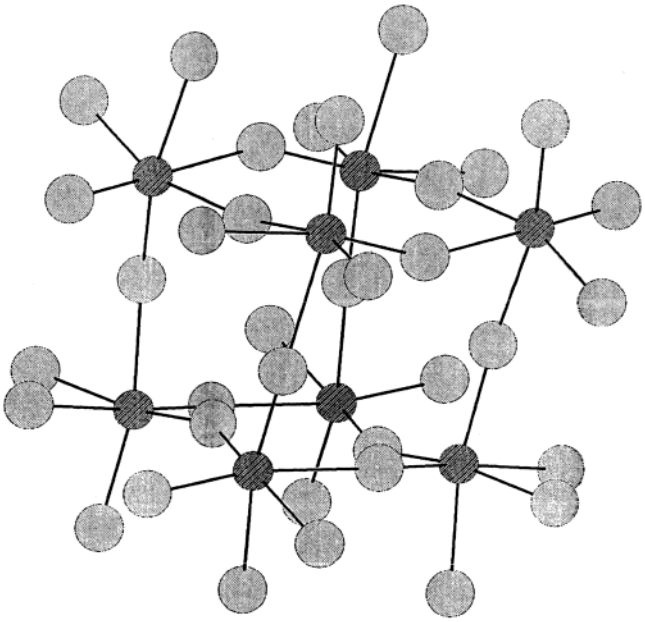

Figure 2. Perovskite type WO_3 structure. Tungsten atoms are illustrated in dark gray while oxygen atoms are depicted in light gray. (Not a unit cell.)

solids has not been unequivocally established. Powder X-ray diffraction results for x mol % V_2O_5−(100 − x) mol % WO_3 materials have suggested the presence of WO_3 crystalline domains for all compositions studied ($10 \leq x \leq 90$). At relatively low V_2O_5 contents ($x \leq 30$), diffraction intensities for V_2O_5 were not observed in contrast to higher V_2O_5 content materials where crystalline V_2O_5 was detected.[6] Diffraction peaks for V_2O_5 were absent at much lower vanadium oxide contents ($x \leq 6-10$) in other X-ray diffraction work suggesting that vanadium oxide is soluble in tungsten oxide to at least 6−10 mol %.[7,8] Powder X-ray diffraction peaks for 10 mol % V_2O_5−90 mol % WO_3 have been assigned to tetragonal WO_3, monoclinic WO_3, and V_2O_5 while qualitative interpretation of ^{51}V magic angle spinning (MAS) NMR suggests the presence of at least two vanadium coordination environments.[9]

In this contribution, vanadium-51 ($I = 7/2$) static and MAS solid-state NMR spectroscopies are employed to elucidate the local atomic environment of vanadium in the x mol % V_2O_5−(100 − x) mol % WO_3 ($10 \leq x \leq 40$) system. All MAS spectra show the full spinning sideband manifold resulting from single quantum excitation of the central and six satellite transitions. We have simulated our MAS and static spectra to obtain chemical shift and quadrupolar tensor parameters. Our interpretation of these parameters and their assignment to vanadium−oxygen bonding environments are discussed.

Experimental Section

Sample Preparation and Characterization. To prepare the vanadium tungsten oxide solids, the appropriate molar ratios of ammonium metavanadate (Aldrich, 99.99% purity) and ammonium polytungstate hydrate (Aldrich, 99.999% purity) were dissolved in hot deionized water. The materials were evaporated to dryness and heated to 500 °C in air for approximately 2 h. The sample of V_2O_5 (Aldrich, 99.99% purity) was used without further purification. Powder X-ray diffraction patterns of the V_2O_5−WO_3 system were obtained using a Scintag X1 powder diffractometer. The diffraction peaks of each sample are broad as previously reported and may be associated with the relatively small particle size of each crystallite.[6,8] The diffraction patterns indicate the presence of V_2O_5 and WO_3 crystalline domains in each sample and are also consistent with previous powder diffraction studies.[6,8,9]

Solid-State NMR. Magic angle spinning ^{51}V NMR spectra were acquired on a Varian Unity Pulse 300 solids spectrometer operating at 78.866 MHz and equipped with a XC-5 MAS probe from Doty Scientific. Samples were packed in the ambient in either silicon nitride or zirconia rotors with Aurum or Kel-F caps. A rotor synchronized echo, $t_p-\tau-t_p-$acquire, with t_p = 1 μs, ν_{rf} = 76.9 kHz, and τ = (spinning speed)$^{-1}$, was used to acquire each MAS spectrum. MAS data for each sample were acquired at two spinning speeds with at least a difference of 1000 Hz to determine the isotropic shift. (Spinning speeds are provided in the appropriate figure caption.) A 0.5-μs dwell time was used to record between approximately 200 and 12800 transients for each sample. A 5-s recycle delay was sufficient to avoid signal saturation. Each time, the domain signal was left-shifted to the echo maximum before apodization and Fourier transformation to provide the frequency domain spectrum.

Single pulse static ^{51}V NMR spectra were acquired on a Varian Unity Plus 300 solids spectrometer operating at approximately 78.866 MHz and equipped with a wide-line probe from Varian. Samples were packed in quartz ampules under ambient conditions. A 1-μs pulse length (ν_{rf} = 62.5 kHz) was used with a 2-μs receiver dead time prior to data acquisition. A 5-s recycle delay was sufficient to avoid signal saturation. A 0.5-μs dwell time was used to record between 1024 and 9000 transients for each sample. All static and MAS spectra are shown referenced to $VOCl_3$(l).

Simulations of the MAS and wide-line ^{51}V spectra were conducted by employing the multipurpose simulation environment of SIMPSON (a general simulation program for solid-state NMR spectroscopy) with MINUIT functions for experimental spectra fitting and uncertainty estimation as described in refs 10 and 11. The determined NMR parameters and their uncertainties reported in Table 1 were obtained by iterative least-squares fits to the ^{51}V MAS data obtained at two spinning speeds for each sample. The isotropic chemical shifts for each sample (δ_{iso}) were determined by obtaining the ^{51}V MAS spectra at two spinning speeds. The value of the isotropic shift was kept fixed during the least-squares fit of the experimental data. MAS spectra exhibiting more than one site were deconvoluted after identification of the isotropic chemical shifts. Each deconvoluted spectrum was iteratively fit. The uncertainties are those reported for fits to the deconvoluted MAS spectra for 20% V_2O_5−80% WO_3 and 10% V_2O_5−90% WO_3. A single-site model was used to fit the MAS spectra of 40% V_2O_5−60% WO_3, 30% V_2O_5−70% WO_3, and V_2O_5. Visual comparisons of experimental and calculated ^{51}V static spectra were also used to derive parameters. The visual inspection allowed more facile identification of the third site parameters for 20% V_2O_5−80% WO_3 and 10% V_2O_5−90% WO_3. The uncertainty reported for the chemical shifts (δ_{iso}) are based on visual inspection of the ^{51}V MAS data.

The following conventions are used. The chemical isotropic shift, shift anisotropy, and asymmetry parameter are, respectively,

$$\delta_{iso} = \frac{1}{3}(\delta_{xx} + \delta_{yy} + \delta_{zz}) \quad (1)$$

$$\delta_{aniso} = \delta_{zz} - \delta_{iso} \quad (2)$$

$$\eta_{cs} = \frac{\delta_{yy} - \delta_{xx}}{\delta_{aniso}} \quad (3)$$

TABLE 1: ^{51}V Chemical Shift Parameters (δ_{iso}, δ_{aniso}, η_{cs}), Quadrupolar Coupling Parameters (C_Q, η_Q), and Relative Tensor Orientations (α, β, γ) for Crystalline V_2O_5 and a Series of Bulk $V_2O_5-WO_3$ Compositions

	δ_{iso} (ppm)	δ_{aniso} (ppm)	η_{cs}	α (deg.)	β (deg.)	γ (deg.)	C_Q (MHz)	η_Q
V_2O_5	-612 ± 1	-639 ± 10	0.1 ± 0.22	62 ± 8	130 ± 13.9	28 ± 14	0.798 ± 0.002	0.2 ± 0.12
40% V_2O_5−60% WO_3	± 1	± 12	± 0.1	± 10	± 11.9	± 8	± 0.012	± 0.12
30% V_2O_5−70% WO_3	± 1	± 13	± 0.11	± 14	± 11.4	± 15	± 0.023	± 0.15
			20% V_2O_5−80% W O3					
site 1	-612 ± 2	-639 ± 12	0.1 ± 0.18	62 ± 13	130 ± 12.4	28 ± 9	0.798 ± 0.037	0.2 ± 0.17
site 2	-584 ± 2	-250 ± 16	0.6 ± 0.14	100 ± 13	105 ± 8	40 ± 11	0.550 ± 0.021	0.7 ± 0.16
site 3	-718 ± 3	-100 ± 15	0	n.d.[a]	n.d.	n.d.	0.100 ± 0.05	0
			10% V_2O_5 –90% WO_3					
site 1	-612 ± 2	-639 ± 16	0.1 ± 0.13	62 ± 9	130 ± 14	28 ± 12	0.798 ± 0.04	0.2 ± 0.19
site 2	-584 ± 2	-250 ± 14	0.6 ± 0.16	100 ± 15	105 ± 7	40 ± 10	0.550 ± 0.04	0.7 ± 0.16
site 3	-718 ± 3	-100 ± 15	0	n.d.[a]	n.d.	n.d.	0.100	0

[a] Coincidence of the chemical shift tensor principal axis system (PAS) and the quadrupole interaction tensor PAS was assumed.

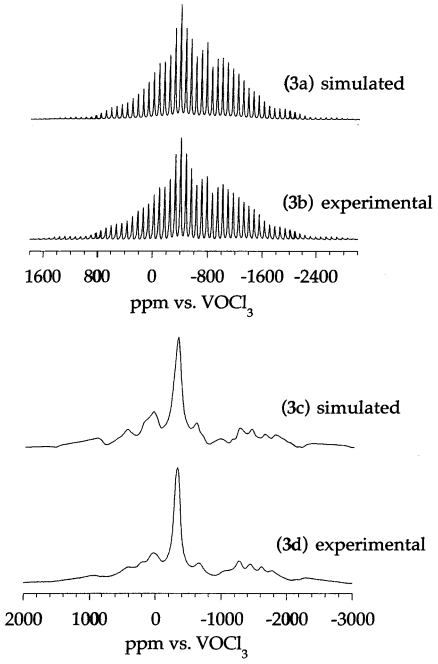

Figure 3. Vanadium-51 NMR spectra of V_2O_5. (a) Simulated MAS NMR spectrum; (b) experimental MAS NMR spectrum; (c) simulated wide-line spectrum; (d) experimental wide-line spectrum. All spectra are referenced to $VOCl_3$. Spectra show single-quantum excitation of the central and all satellite transitions. MAS spinning speed, $\nu_{rot} = 6025$ Hz.

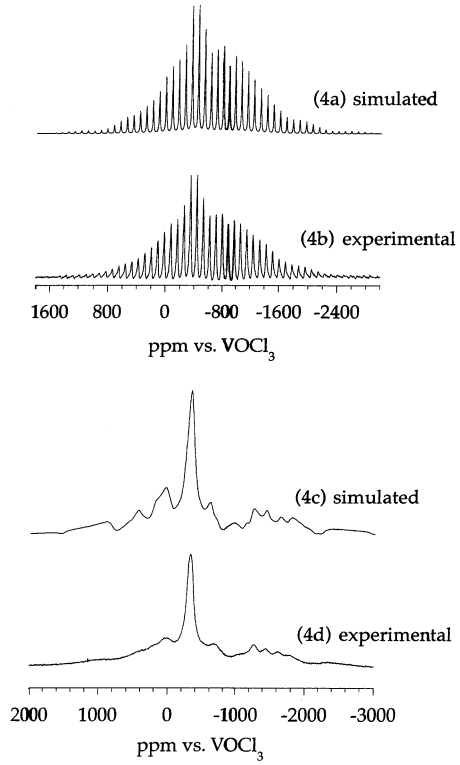

Figure 4. Vanadium-51 NMR spectra of nominally 40 mol % V_2O_5−60 mol % WO_3. (a) Simulated MAS NMR spectrum; (b) experimental MAS NMR spectrum; (c) simulated wide-line spectrum; (d) experimental wide-line spectrum. All spectra are referenced to $VOCl_3$. Spectra show single-quantum excitation of the central and all satellite transitions. MAS spinning speed, $\nu_{rot} = 7060$ Hz.

with the principal elements of the chemical shift tensor ordered as $|\delta_{zz} - \delta_{iso}| \geq |\delta_{xx} - \delta_{iso}| \geq |\delta_{yy} - \delta_{iso}|$. The quadrupolar coupling constant and quadrupolar asymmetry parameter are given as

$$C_Q = \frac{e^2Qq}{h} \tag{4}$$

$$\eta_Q = \frac{V_{yy} - V_{xx}}{V_{zz}} \tag{5}$$

Results

Shown in Figure 3 are the experimental and simulated MAS and static spectra of V_2O_5. Our ^{51}V MAS spectrum of V_2O_5 is consistent in appearance with previously reported MAS spectra of the central and satellite transition spinning sideband manifolds.[12−14] However, differences in our observed sideband intensities and relative positions are likely due to the different spinning speeds and field strengths employed in previous studies. Spectral parameters from simulated MAS and static are provided in Table 1. With the exception of the orientation of the chemical shift tensor principal axis system (PAS) with respect to the quadrupole tensor PAS, all spectral parameters are identical, within experimental error, to previously determined parameters.[12−14] However, differences among the reported Euler angles, including our present determination, may be due to the small influence of the relative tensor orientations when either η_{cs} or η_Q are close to zero.

The MAS and static spectra of 40 mol % V_2O_5−60 mol % WO_3 and 30 mol % V_2O_5 −70 mol % WO_3 are nearly identical to each other and are shown in Figures 4 and 5, respectively. The spectral parameters are quite similar to those for bulk crystalline V_2O_5 as reported in Table 1. Differences between the static spectra of x mol % V_2O_5− (100 − x) mol % WO_3 ($x = 30$, 40) and V_2O_5 will be addressed in the Discussion section. Figures 6 and 7 show experimental and simulated spectra for 20 mol % V_2O_5−80 mol % WO_3 and 10 mol %

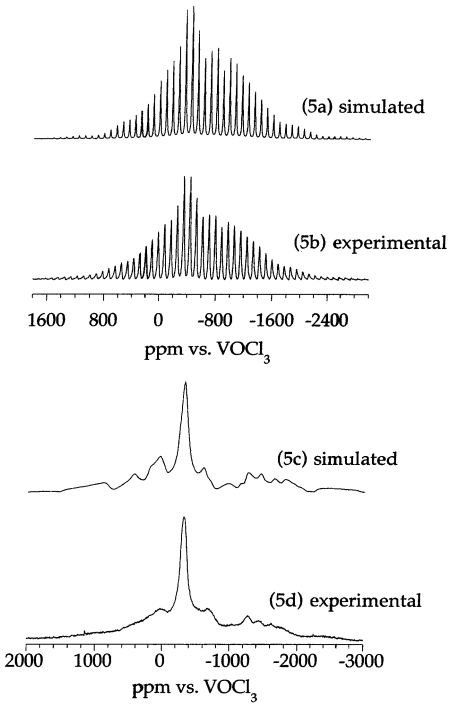

Figure 5. Vanadium-51 NMR spectra of nominally 30 mol % V_2O_5−70 mol % WO_3. (a) Simulated MAS NMR spectrum; (b) experimental MAS NMR spectrum; (c) simulated wide-line spectrum; (d) experimental wide-line spectrum. All spectra are referenced to $VOCl_3$. Spectra show single-quantum excitation of the central and all satellite transitions. MAS spinning speed, ν_{rot} = 7029 Hz.

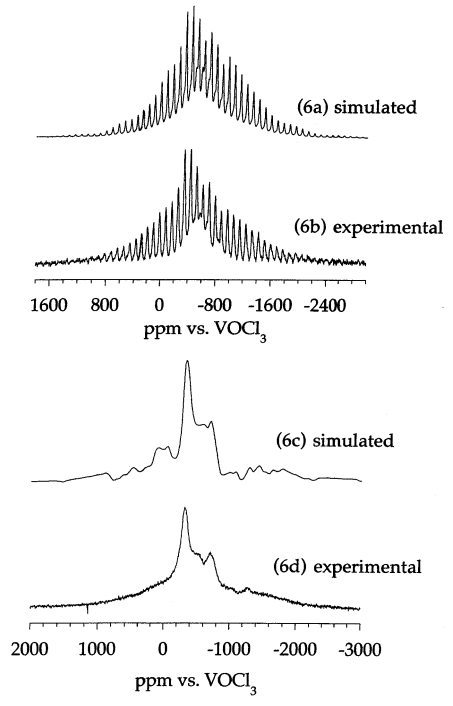

Figure 6. Vanadium-51 NMR spectra of nominally 20 mol % V_2O_5−80 mol % WO_3. (a) Simulated MAS NMR spectrum; (b) experimental MAS NMR spectrum; (c) simulated wide-line spectrum; (d) experimental wide-line spectrum. All spectra are referenced to $VOCl_3$. Spectra show single-quantum excitation of the central and all satellite transitions. MAS spinning speed, ν_{rot} = 7000 Hz.

V_2O_5−90 mol % WO_3, respectively. The ^{51}V MAS and static spectra of 10 mol % V_2O_5−90 mol % WO_3 show the larger intensity of site 2 at the expense of site 1. Spectral parameters for a three-site model are provided in Table 1 and the relative

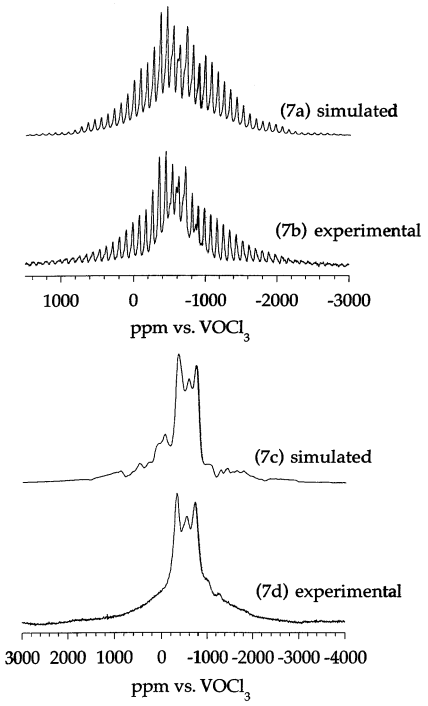

Figure 7. Vanadium-51 NMR spectra of nominally 10 mol % V_2O_5−90 mol % WO_3. (a) Simulated MAS NMR spectrum; (b) experimental MAS NMR spectrum; (c) simulated wide-line spectrum; (d) experimental wide-line spectrum. All spectra are referenced to $VOCl_3$. Spectra show single-quantum excitation of the central and all satellite transitions. MAS spinning speed, ν_{rot} = 7090 Hz.

TABLE 2: Relative Site Occupancies for Bulk V_2O_5−WO_3 Solids Determined from Simulation of ^{51}V MAS and Static Solids NMR Spectra[a]

sample	site 1	site 2	site 3
40% V_2O_5−60% WO_3	100%		
30% V_2O_5−70% WO_3	100%		
20% V_2O_5−80%WO_3	79.5 ± 3.5%	17 ± 3%	3.5 ± 0.5%
10% V_2O_5−90%WO_3	68.5 ± 3.5%	28 ± 3%	3.5 ± 0.5%

[a] Sample percentages are given as nominal mole %.

contribution of each site to the intensity of the MAS or static spectrum is shown in Table 2.

Discussion

The crystalline vanadates exhibit a variety of vanadium coordination environments that give rise to distinct ^{51}V chemical shift anistropies in the solid state. Briefly, isolated VO_4^{3-} tetrahedra are typically observed in orthovanadates and give rise to typical ^{51}V chemical shift anisotropies ($\delta_{aniso} = \delta_{zz} - \delta_{iso}$) of |30| to |100| ppm consistent with the nearly spherically symmetric oxygen coordination of the vanadium.[15] Discrete $[V_2O_7]^{4-}$ units, found in pyrovanadates, are formed from two-corner-shared VO_4^{3-} tetrahedra. The distortion of each VO_4^{3-} tetrahedron gives rise to chemical shift anisotropies in the range of |100| to |250| ppm.[16] Infinite chains of corner-shared four-coordinate vanadium are found in metavanadates where the deviation from tetrahedral symmetry is reflected by typical chemical shift anisotropies of |190| to |315| ppm.[15,17] The solid state ^{51}V NMR of vanadium of distorted octahedral or five-coordinate environments in pyro- and metavanadates as well as V_2O_5 show large chemical shift anisotropies which range from |295| to |640| ppm.[12,17]

Quadrupolar coupling constants and quadrupolar asymmetry parameters of crystalline model compounds may show large

variations of C_Q or η_Q among isomorphous vanadium compounds.[15,18] Quadrupolar coupling constants of $C_Q = 2.95$ and 4.20 MHz were observed for the isostructural NH_4VO_3 and KVO_3. However, the differences among vanadium−oxygen bond distances are identical within experimental error, while the oxygen−vanadium−oxygen bond angles differ by about 1−4°.[19] The reported quadrupolar asymmetry parameters for the isomorphous $Mg_3(VO_4)_2$ and $Zn_3(VO_4)_2$ are, respectively, $\eta_Q = 0.56$ and 0.99. Yet, the vanadium−oxygen bond distances and oxygen−vanadium−oxygen bond angles in $Mg_3(VO_4)_2$ range from 1.695 to 1.809 Å and 108.30° to 110.51°,[20] while the vanadium−oxygen bond distances and oxygen−vanadium−oxygen bond angles in $Zn_3(VO_4)_2$ range from 1.703 to 1.814 Å and 107.99° to 111.12°.[21] It is possible that the second or third coordination spheres of atoms surrounding the vanadium influences the quadrupolar tensor elements. However, to the best of our knowledge, no such systematic studies have been reported in the literature. Thus, the chemical shift anisotropy, δ_{aniso}, is currently a better parameter to consider in a structural analysis than the quadrupolar coupling constant, C_Q, or quadrupolar asymmetry parameter, η_Q. Also, an unequivocal structural interpretation of solid state ^{51}V isotropic chemical shifts, δ_{iso}, has not been established.[22]

The static spectra of 40 mol % V_2O_5−60 mol % WO_3 and 30 mol % V_2O_5−70 mol % WO_3 are similar to that of V_2O_5 and a reasonable fit is achieved using a single-site model utilizing the spectral parameters of V_2O_5 as initial parameters for the fit. However, it is clear that spectral features to the high frequency and to a slightly lesser degree the low-frequency side of the static spectrum maximum at −306 ppm lack the distinct characteristics observed in the static spectrum of crystalline V_2O_5. A distribution of quadrupolar coupling constants, C_Q, of about 150 kHz results in a smoothing of the more distinct static spectral features to the low- and high-frequency side of the static spectrum maximum at −306 ppm with little change to the maximum position or width.[14] This is to be expected since the maximum intensity at −306 ppm primarily results from the central transition (±1/2) which is less sensitive to quadrupolar broadening when the chemical shift interaction is relatively larger than the quadrupolar interaction.

The effect of a distribution of quadrupolar coupling constants is less apparent in the MAS spectra of 40 mol % V_2O_5−60 mol % WO_3 and 30 mol % V_2O_5 −70 mol % WO_3. A Gaussian distribution of quadrupolar coupling constants ($\Delta C_q = 150$ kHz) very slightly affects the relative intensities of the outer MAS sidebands arising from the single quantum satellite transitions with largest |m| at spinning speeds of 2000 Hz.[14] However, the relative intensities of the |7/2| to |5/2| and |5/2| to |3/2| satellite transition sidebands contribute less to the total spectrum at the spinning speeds (6000−7000 Hz) employed in our study. One, therefore, might not expect a C_Q distribution to drastically alter the relative intensities of the MAS spinning sideband manifold.

It is also possible that a distribution of tensor orientation angles or quadrupolar asymmetry parameters ($\Delta\eta_Q$ about 0.3) smooths the low- and high-frequency spectral features of the static spectra. Since the chemical shift and quadrupolar PAS are fixed to the molecule, we might expect that a distribution of tensor orientation angles would also manifest itself in a distribution of the chemical shift parameters. However, it is less likely that large distributions of the isotropic chemical shift or anisotropic chemical shift parameter exist since variations of the chemical shift tensor elements (e.g., variation of δ_{aniso} by ±50 ppm) lead to gross changes in the overall spectral width and peak maximum at −306 ppm. Additionally, a Gaussian distribution of isotropic shifts as small as $\Delta\delta_{iso} = 10$ ppm or $\Delta\delta_{aniso} = 20$ ppm would likely lead to significant changes in the appearance of the MAS sideband manifold.[14] However, smaller distributions of the shift tensor elements may also be present.

The MAS and static spectra of 10 mol % V_2O_5−90 mol % WO_3 and 20 mol % V_2O_5−80 mol % WO_3 are more complex than those of 40 mol % V_2O_5−60 mol % WO_3 and 30 mol % V_2O_5−70 mol % WO_3. Our simulations of both MAS and static spectra indicate the presence of three vanadium coordination environments. The three isotropic resonances were determined by comparing MAS spectra obtained at two spinning speeds that differed by about 1000 Hz. Spectral parameters for site 1 are quite similar to those obtained for crystalline V_2O_5 suggesting the presence of a square pyramid type arrangement of oxygen atoms around the vanadium. The chemical shift anisotropy of site 2 is −250 ppm (Table 1) and is within the range of shift anisotropies reported for corner-shared vanadium atoms in distorted tetrahedral coordination environments. The relatively large chemical shift asymmetry parameter, $\eta_{cs} = 0.6$, suggests a deviation of the local oxygen coordination from axial symmetry. The vanadium coordination of site 3 is likely to be spherically symmetric as suggested by the relatively small chemical shift anisotropy parameter presented in Table 1 and is within range of observed shift anisotropies for crystalline compounds containing isolated vanadium−oxygen tetrahedra. The assignment of site 3 to a spherically symmetric site is also consistent with the determined chemical shift asymmetry parameter, η_{cs}, of zero, and the small quadrupolar coupling constant and quadrupolar asymmetry parameter.

Similar to the static spectra of 40 mol % V_2O_5−60 mol % WO_3 and 30 mol % V_2O_5−70 mol % WO_3, the static spectra of 20 mol % V_2O_5−80 mol % WO_3 and 10 mol % V_2O_5−90 mol % WO_3 lack the distinct spectral features from about 0 to 1000 ppm and −1000 to 2000 ppm. Again, the smoothing of these features in the experimental static spectrum is attributed to a distribution of quadrupolar coupling constants ($\Delta C_q = 150$ kHz) or quadrupolar asymmetry parameters ($\Delta\eta_Q = 0.3$). Such a distribution of spectral parameters may suggest vanadium−oxygen bond angle and bond length distributions or variations in the second and higher vanadium coordination spheres. A systematic study correlating ^{51}V solid-state NMR spectral parameters with outer and the first vanadium−oxygen coordination spheres may provide further insight.

Conclusions

A single vanadium site was observed in the nominally 40 mol % V_2O_5−60 mol % WO_3 and 30 mol % V_2O_5−70 mol % WO_3 compositions. Interpretation of NMR spectral parameters suggests that the vanadium in this single site resides in a square pyramid-like oxygen coordination environment. Three sites were observed for the nominally 20 mol % V_2O_5−80 mol % WO_3 and 10 mol % V_2O_5−90 mol % WO_3 compositions. The spectral parameters for the three sites are consistent with the presence of vanadium(V) in (1) square pyramid-like, (2) distorted tetrahedral, and (3) spherically symmetric oxygen coordination environments. A distribution of ^{51}V quadrupolar coupling parameters may be present and may suggest a distribution of second or higher order atomic coordination environments. Similar to vanadates containing mono- and divalent metals, such as $K_3V_5O_{14}$, $Tl_3V_5O_{14}$, and $Hg_4V_2O_9$, the coexistence of five- and four-coordinate vanadium environments in a polycrystalline material are observed in the vanadium−tungsten oxide compositions examined in this study. The results of this present

contribution may provide useful insights into the vanadium coordination environments on supported $V_2O_5-WO_3/TiO_2$ catalysts.[23]

Acknowledgment. B.G. thanks Professor Ruth Stark and Dr. Hsin Wang (Department of Chemistry, College of Staten Island, City University of New York) for use of their solid-state NMR instrumentation. Partial support of this work was provided by the Faculty Scholarship and Development Committee (Brooklyn Campus), the Vice President of Academic Affairs, and the Trustees of Long Island University. Acknowledgment is made to the donors of the Petroleum Research Fund, administered by the American Chemical Society for partial support of this research (ACS-PRF No. 34967-GB5).

References and Notes

(1) Bosch, H.; Janssen, F. *Catal. Today* **1988**, *2*, 369.
(2) Ramis, G.; Busca, G.; Forzatti, P. *Appl. Catal. B* **1992**, *1*, L9.
(3) Rougier, A.; Blyr, A.; Quédé, A. *J. Electrochem. Soc.* **2001**, *148*, H7.
(4) Enjalbert, R.; Galy, J. *Acta Crystallogr.* **1986**, *C42*, 1467.
(5) Loopstra, B. O.; Boldrini, P. *Acta Crystallogr.* **1966**, *21*, 158.
(6) Satsuma, A.; Hattori, A.; Mizutani, K.; Furuta, A.; Miyamoto, A.; Hattori, T.; Murakami, Y. *J. Phys. Chem.* **1988**, *92*, 6052.
(7) Yan, Z.; Andersson, S. L. T. *Appl. Catal.* **1990**, *66*, 149.
(8) Inglot, A.; Najbar, M.; Borzecka-Prokop, B. *J. Chem. Soc., Faraday Trans.* **1995**, *91*, 145.
(9) Najbar, M.; Camra, J.; Bialas, A.; Weselucha-Birczynska, A.; Brozecka-Prokop, B.; Delevoye, L.; Klinowski, J. *Phys. Chem. Chem. Phys.* **1999**, *1*, 4645.
(10) Bak, M.; Rasmussen, J. T.; Nielsen, N. C. *J. Magn. Reson.* **2000**, *147*, 296.
(11) James, F. *Minuit Function Minimization and Error Analysis Version Reference Manual 94.1*; CERN Program Library Office: Geneva, Switzerland, 1998.
(12) Skibsted, J.; Nielsen, N. C.; Bildsøe, H.; Jakobsen, H. J. *Chem. Phys. Lett.* **1992**, *188*, 405.
(13) Marichal, C.; Kempf, J.-Y.; Maigret, B.; Hirschinger, J. *Solid State NMR* **1997**, *8*, 33.
(14) Shubin, A. A.; Lapina, O. B.; Bosch, E.; Spengler, J.; Knözinger, H. *J. Phys. Chem.* **1999**, *103*, 3138.
(15) Skibsted, J.; Jacobsen, C. J. H.; Jakobsen, H. J. *Inorg. Chem.* **1998**, *37*, 3083.
(16) Nielsen, U.; Jakobsen, H. J.; Skibsted, J. *J. Phys. Chem. B* **2001**, *105*, 420.
(17) Nielsen, U.; Jakobsen, H. J.; Skibsted, J. *Inorg. Chem.* **2000**, *39*, 2135.
(18) Skibsted, J.; Nielsen, N. C.; Bildsoe. H.; Jakobsen, H. *J. Am. Chem. Soc.* **1993**, *115*, 7351.
(19) Hawthorne, F. C.; Calvo, C. *J. Solid State Chem.* **1977**, *22*, 157.
(20) Krishnamachari, N.; Calvo, C. *Can. J. Chem.* **1971**, *49*, 1629.
(21) Nord, A. G.; Åberg, G.; Stefanidis, T.; Kiekegaard, P.; Grigoriadis, V. *Chem. Scr.* **1985**, *25*, 212.
(22) Eckert, H.; Wachs, I. E. *J. Phys. Chem.* **1989**, *93*, 6796.
(23) Gheorghe, C.; Gee, B. *Chem. Mater.* **2000**, *12*, 682.